ELSEVIER

Surface Science 421 (1999) 308–319

surface science

On the commensurate–incommensurate transition in adsorbed monolayers

A. Patrykiejew [a,*], S. Sokołowski [a], T. Zientarski [a], K. Binder [b]

[a] *Faculty of Chemistry, MCS University, 20031 Lublin, Poland*
[b] *Institut für Physik, Johannes-Gutenberg-Universität Mainz, 55099 Mainz, Germany*

Received 29 June 1998; accepted for publication 2 November 1998

Abstract

A Monte Carlo simulation method is used to study the commensurate–incommensurate phase transition in monolayers and the formation of bilayer films on the (100) face of an fcc crystal. The phase diagram for the system which forms the registered (1×1) and high density incommensurate phases in the monolayer has been determined. It is shown that the registered phase undergoes the transition to a denser incommensurate solid phase when the film density increases. The mechanism of melting of the monolayer film is found to depend on the film density. In particular, the melting of dense incommensurate solid monolayer film is found to be accompanied by the transfer of adsorbed molecules into the second layer. © 1999 Published by Elsevier Science B.V. All rights reserved.

Keywords: Adsorption; Monte Carlo simulation; Phase transitions

1. Introduction

One of the most interesting features of monolayer films adsorbed on crystal surfaces is the formation of various ordered phases during adsorption [1–5]. The actual structure of the adsorbed layer depends on many factors. Chief among these are the properties of the surface potential, the symmetry of the substrate surface and the relative size of the adsorbate atoms and the surface unit lattice cell. Of course, the external thermodynamic conditions, such as the film density, its chemical potential and temperature, considerably influence the film structure as well.

When the surface potential exhibits sufficiently large periodic variations in directions parallel to the surface, the adsorbed films usually form epitaxial structures at low temperatures. Such commensurate phases can be conveniently described in the framework of various lattice gas models [6–11]. Another limiting situation corresponds to the systems with very weak periodicity of the gas–solid potential. In such cases, the monolayer can be considered as a two-dimensional (2D) uniform system and the properties of the adsorbed film can be evaluated using appropriately modified theories of bulk uniform matter, such as the density functional theory [12,13] and various integral equation approaches [14–16].

The most complex situation appears for moderately corrugated surfaces, when the potential barriers between adjacent sites are comparable with the effects due to the admolecule–admolecule interaction. Competition between the periodic surface field and the admolecule–admolecule interaction may lead to the formation of both commensurate

* Corresponding author.

0039-6028/99/$ – see front matter
PII: S0039-6028(98)00858-9

and incommensurate phases. Their regions of stability depend on the film density and temperature [17–25].

The most often invoked picture of incommensurate phases relies on the concept of domain walls [26–30], which separate large regions of nearly commensurate phase. The best known, and most intensively studied systems exhibiting both commensurate and incommensurate phases, are rare gas monolayers on graphite [2,31–36], as well as monolayers formed on the (110) face of metals [24,37–40]. In all experimentally studied systems, the adsorbate atoms are too large for the occupation of adjacent lattice sites. For example, krypton, helium, or hydrogen adsorbed on graphite form the $\sqrt{3}\times\sqrt{3}$ registered phase with threefold degeneracy. Xenon adsorbed on the (110) face of copper orders into the $c(2\times2)$ phase, which exhibits twofold degeneracy. The above examples illustrate the class of systems exhibiting the commensurate–incommensurate transition which, in general, can be described using the domain wall formalism [28]. The validity of the domain wall theory is limited to the so-called weakly incommensurate (WIC) systems with degenerated commensurate ground state. When the density of the incommensurate phase increases, the domain walls become increasingly broader, so that for sufficiently high density they eventually start to overlap. The resulting high density solid phase (HIC), often called a "floating 2D solid phase" [41], exhibits properties quite different than the weakly incommensurate phase with domain walls. Namely, the role of the substrate potential in HIC is merely to 'pin' the monolayer to the solid surface. In such systems, the only effect of the gas–solid potential periodicity is usually a small rotation of the film with respect to the surface lattice [42–46]. The domain wall description also cannot be applied to systems with a nondegenerated commensurate ground state, as occurs for monolayers exhibiting the (1×1) ordered structure. The mechanism of melting for WIC and HIC phases is quite different [41,47,48].

Here we present the results of a Monte Carlo study of a phase diagram for a simple system of particles adsorbed on the (100) plane of the face-centred cubic (fcc) crystal. We assume that the adsorbed particles are small enough to allow for mutual occupancy of adjacent potential minima (adsorption sites) and consider the regime of monolayer and bilayer adsorption.

The primary goal of our work has been to extend the scope of our former study [49] to systems of higher density, well above the density of the epitaxial (1×1) phase, and explore the phase diagram for the system expected to exhibit the registered as well as the high density incommensurate phases in the first layer. Also, we consider the changes in the mechanism of melting transition in monolayer films of different density. In particular, we discuss the possibility of the second layer promotion which results from the melting of a dense monolayer solid. Finally, we tackle the problem of possible changes in the first layer structure due to the condensation of the second layer. Such monolayer–bilayer equilibria have been studied theoretically by Bruch and Wei [50,51], but only in the case of films formed on substrates with negligible periodicity of the gas–solid potential.

The organization of this paper is as follows. In Section 2 we present the interaction potentials which specify our model and describe the system studied here. Then, in Section 3 we discuss briefly the simulation methods used. The results of our study are presented and discussed in Section 4. In Section 5 we summarize briefly our findings.

2. The model

The model considered here is essentially the same as used in Ref. [49]. Thus, we assume that the surface is a perfect (100) plane of the fcc crystal. In general, the potential representing the interaction between the adsorbate atom and the surface is given by the well-known Fourier expansion [52]

$$v(z,\boldsymbol{\tau})=\sum_{q} v_{\boldsymbol{q}}(z)\exp(-\mathrm{i}\boldsymbol{q}\cdot\boldsymbol{\tau}) \tag{1}$$

where the Fourier coefficients $v_{\boldsymbol{q}}(z)$ are the functions of the distance from the surface z, $\boldsymbol{\tau}=(x,y)$ is the 2D vector specifying the position of the adsorbate atom over the surface and the summa-

tion runs over all reciprocal surface lattice vectors $\boldsymbol{q}$. Here we assume a slightly modified form of the gas–solid potential [49,53]

$$v(z,\boldsymbol{\tau})=\epsilon_{gs}\left[v_o(z)+V_b\sum_{\boldsymbol{q}\neq 0}v_{\boldsymbol{q}}(z)f_{\boldsymbol{q}}(\boldsymbol{\tau})\right] \quad (2)$$

in which the periodic part can be varied by appropriate choice of the parameter V_b, which we shall call the corrugation coefficient. When V_b is equal to unity, Eq. (2) becomes identical with Eq. (1). The explicit forms of the Fourier coefficients $v_{\boldsymbol{q}}(z)$ and the functions $f_{\boldsymbol{q}}(\boldsymbol{\tau})$ can be found in Ref. [52]. In particular, the functions $f_{\boldsymbol{q}}(\boldsymbol{\tau})$ are defined as

$$f_{\boldsymbol{q}}(\boldsymbol{\tau})=\cos(|\boldsymbol{q}_1|x)\cos(|\boldsymbol{q}_2|y) \quad (3)$$

where $|\boldsymbol{q}_1|$ and $|\boldsymbol{q}_2|$ are the lengths of the components of the reciprocal vector $\boldsymbol{q}$.

In general we consider systems with the corrugation coefficient not exceeding unity, since for higher values of V_b the series Eq. (2) does not properly describe the gas–solid potential for small distances from the surface. Calculations of the potential $v(z,\boldsymbol{\tau})$ have been carried out including only the first five terms in the series Eq. (2) [49,52].

The gas–gas interaction is represented by a standard (12−6) Lennard–Jones potential

$$u(r)=4\epsilon_{gg}\left[\left(\frac{\sigma_{gg}}{r}\right)^{12}-\left(\frac{\sigma_{gg}}{r}\right)^{6}\right] \quad (4)$$

truncated at a certain cut-off distance r_{max}, and we have assumed here that $r_{max}=3\sigma$.

In this paper we study the properties of just one system of particles with the diameter $\sigma^*=\sigma_{gg}/a=0.8$, where a is the surface lattice constant. Although Eq. (4) can be related to physical parameters of real systems easily – e.g. for the rare gas Kr we would have $\epsilon_{gg}=160$ K, $\sigma_{gg}=3.60$ Å and hence a reduced temperature $T^*=1$ then would correspond to 160 K – the choice for $\sigma^*=\sigma_{gg}/a=0.8$ is nothing but an illustrative model assumption. We do not intend to model faithfully a particular system here, but rather want to elucidate the generic features due to such length scale misfit. The parameters determining the strength and the periodicity of the gas–solid potential, $\epsilon^*_{gs}=\epsilon_{gs}/\epsilon_{gg}$ and V_b, have also been fixed and assumed to be equal to $\epsilon^*_{gs}=2.0$ and $V_b=0.8$. The values of the gas–solid potential minima corresponding to different locations of an atom over the lattice cell and the potential barrier for translation corresponding to the system considered in this work are summarized in Table 1. The choice of the parameters have been guided by the results of our earlier studies [49]. Namely, from the ground-state calculations as well as from the results of Monte Carlo simulation performed for the same system at the number density $\rho_n=1.0$ (here, the number density is defined as the ratio N/M, where N is the number of adsorbate atoms in the film and M the number of surface unit cells) it follows that the low temperature stable phase is the commensurate (1×1) structure. When the parameter V_b becomes lower than about 0.7 the stable low temperature phase corresponds to the hexagonal close-packed structure, which forms compact islands with a clearly seen uniaxial ordering. One can suspect that, in the case of $V_b=0.8$, the stability of the registered phase would be limited to a certain range of densities and temperatures, however. An increase in the film density (or the chemical potential of the adsorbate) may either trigger the commensurate–incommensurate transition within the first layer or cause a gradual formation of the second layer on top of the commensurate phase in the first layer.

The primary goal of the present work has been just to determine the behaviour of the adsorbed film over a range of densities (above the density of the epitaxial (1×1) phase) and temperatures.

3. Methods

The study has been carried out with the help of continuous space Monte Carlo simulations per-

Table 1
The locations and values of the gas–solid potential minima for different locations of the adsorbate atom over the lattice cell

$\boldsymbol{\tau}$	$z_{min}(\boldsymbol{\tau})$	$V^*_{min}[z_{min}(\boldsymbol{\tau})]$
(0.0, 0.0)	0.957	−6.398
(0.5, 0.0)	0.858	−8.167
(0.5, 0.5)	0.802	−9.349

$V^*_{min}[z_{min}(0.5, 0.0)]-V^*_{min}[z_{min}(0.5, 0.5)]=1.182$

formed in the canonical and the grand canonical ensembles. In both cases we have used the same, three-dimensional simulation cells of the size $M_x \times M_y \times M_z$. The crystal surface (or rather a top layer of atoms of the crystal lattice) has been located at $z=0$ and the standard periodic boundary conditions have been applied in both x and y directions. At $z=M_z$ we have placed a simple reflecting hard wall. In this work we have set $M_z=10$, with the surface unit lattice cell constant a used as a length unit. At low temperatures, and when the film thickness does not exceed two or three atomic layers, the nature of the system closure at $z=M_z$ is irrelevant owing to the extremely low bulk density $\rho_{n,b}$. The bulk densities have been estimated by a direct summation of the particles located at the distances from the solid surface exceeding the region corresponding to the surface layer. The region of z corresponding to the adsorbed film varies, of course, with temperature and the chemical potential. At all temperatures and the total densities of the adsorbate considered here, the adsorbed layer thickness has never exceeded three atomic layers and the bulk density has been very low (not higher than $\rho_{n,b} \approx 5 \times 10^{-3}$) and uniform over a wide range of distances from the surface. The size of the simulation cell in the x and y directions has been varied and assumed the values equal to 16, 20, 40 and 60 units.

The canonical ensemble simulation (CMC) has been done in the same way as described in Ref. [49], using the list of neighbours and the dynamical adjustment of the maximum allowed jump length, to keep the acceptance ratio of about one-half. The number of Monte Carlo moves ranged between 10^8 and 5×10^9, depending on the film density and temperature. An additional 10^7–10^8 moves were used for equilibrating the system. Usually, the starting configuration was obtained by placing the assumed number of particles in random positions over the surface. Then the system was equilibrated at a high temperature of the order $T^*=kT/\epsilon_{gg}=1.0$. Subsequently, the temperature was gradually lowered to the lowest value of 0.01 considered here. After freezing, the system was heated gradually, in order to check whether the observed changes in its properties were reversible.

In the case of grand canonical simulation (GCMC) we have used the standard algorithm [54–56] and assumed that the activity is expressed by

$$\gamma = (h^2/2\pi mkT)^{-3/2} \exp(\mu^*/T^*) \quad (5)$$

where the reduced chemical potential is given by $\mu^*=\mu/\epsilon_{gg}$, and the pre-exponential factor has been approximated as $T^{*3/2}$. Usually, the runs at a given temperature were initiated assuming a sufficiently low value of the chemical potential, which corresponds to the 2D gas phase and very low adsorption.

The basic recorded quantities were the gas–gas and the gas–solid interaction energies (per particle), the heat capacity (from the fluctuation theorem) and the local density profiles. In addition, we also performed the analysis of Voronoi polygons [53,57]. In this way it was possible to monitor the changes in the inner structure of the adsorbed layers and to calculate the average nearest neighbour distance as well as the average misfit with respect to the registered structure. In some cases, we have also performed the calculations of the block density probability distributions [58–60]. This method is particularly well suited for detection of the two-phase coexistence in the CMC simulation. Of course, in order to obtain reliable results it is necessary to use sufficiently large systems. In this work, we have used a simulation cell of size $60 \times 60 \times 10$ containing 4000 particles.

4. Results and discussion

Fig. 1 presents a series of adsorption–desorption isotherms obtained from the GCMC simulation. At sufficiently low temperatures we observe discontinuities connected with the first-order phase transitions. It should be emphasized here that the actual adsorption–desorption isotherms obtained at low temperatures exhibit pronounced hysteresis loops due to metastability effects. The isotherms plotted in Fig. 1 have been obtained by placing the vertical lines at the middle points of the hysteresis loops. The first step in the isotherms corresponds to condensation of the 2D gas into the registered 1×1 phase. At low temperatures the

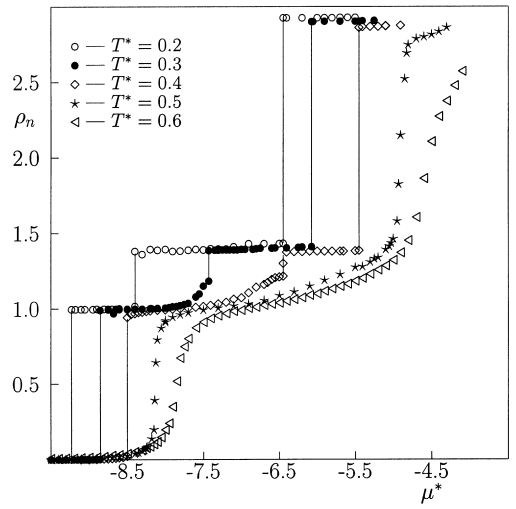

Fig. 1. Adsorption isotherms obtained from the GCMC simulation at different temperatures for systems of size $20\times20\times10$.

dilute gas phase behaves as a nearly perfect lattice gas, whereas at higher temperatures the particles start to wander over the surface. Anyway, the transition between the gas and the registered (1×1) phase is expected to belong to the universality class of the 2D Ising ferromagnet [61]. In this case, our assumption that the transition points are located at the middle points of the hysteresis is justified, owing to the particle–hole symmetry of the system undergoing the transition from the 2D (lattice) gas to the (1×1) registered phase.

A striking feature of the adsorption isotherms obtained at low temperatures and presented in Fig. 1 is a clear indication of the first-order commensurate–incommensurate phase transition. In Fig. 2a and b we show the examples of configurations for both the commensurate and the incommensurate phases at $T^*=0.2$, and in Fig. 2c the density profiles characteristic for both solid phases are shown. It is evident that the dense incommensurate phase is hexagonally ordered and slightly rotated with respect to the substrate lattice. Since this system exhibits quite large periodic variations of the gas–solid potential, the locations of the adsorbed particles in the incommensurate phase show pronounced deviations from planarity (see Fig. 2c). From the data given in Table 1 it is evident that the equilibrium distance from the

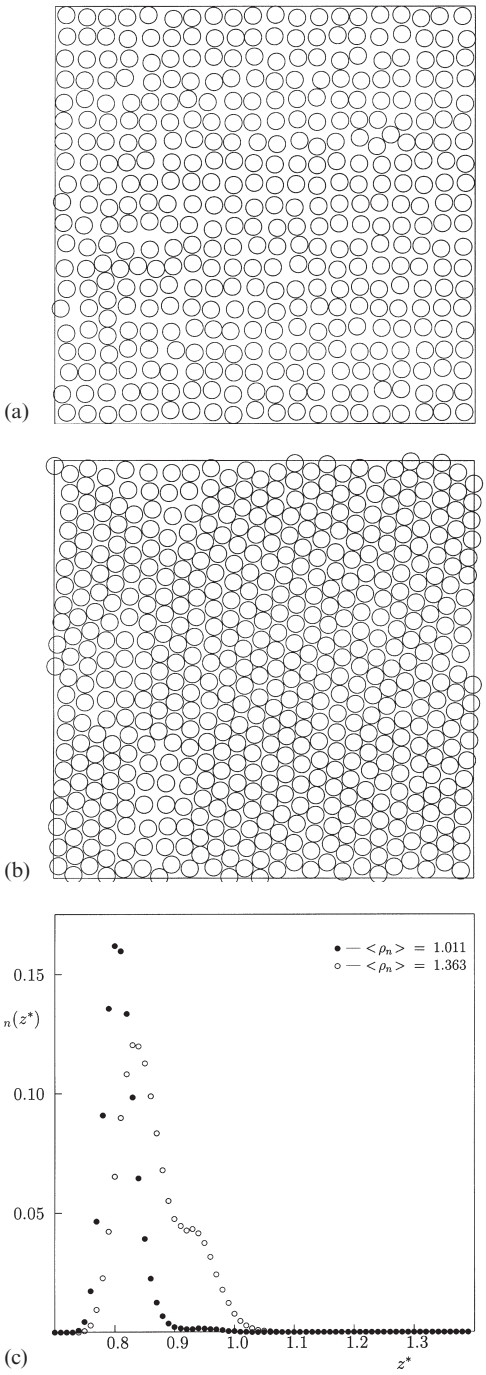

Fig. 2. Snap-shot configurations (a) and (b) recorded at $T^*=0.2$ and the chemical potential $\mu^*=-8.45$ on both sides of the commensurate (a)–incommensurate (b) transition. (c) The corresponding local density profiles (averaged over the surface) for both phases.

surface exhibits large variations when the adsorbed atom assumes different positions within the surface cell. The incommensurate phase has been found to change its orientation with respect to the surface lattice with temperature, though we have not attempted any quantitative estimation of this effect.

The approach developed by Novaco and McTague [42,43] is not appropriate for the system considered as it assumes that the film is strictly 2D. In principle, a much more suitable approach to the problem of epitaxial rotation in the system studied in this work might be the theory proposed by Vives and Lindgård [62]. Its application, however, would require much larger systems than those used here, as well as a careful analysis of the effects of finite size and of the system's shape. The properties of the dense incommensurate phase in the monolayer film allow us to assume that this phase is a floating solid. It is noteworthy that the transition leading to the formation of that dense floating solid phase appears to change its mechanism with temperature. Only at temperatures not exceeding about 0.2, is the low density phase a nearly perfect registered structure. At higher temperatures we find a continuous increase in the density with the chemical potential, below the value at which the first-order transition occurs. In Fig. 3 we show an example of the system configuration recorded at $T^*=0.3$ and $\mu^*=-7.5$, just below the point of the first-order transition. It is clearly seen that there are domains of the (1×1) phase, the domain exhibiting hexagonal ordering, as well as lots of defects.

The isotherms shown in Fig. 1 also demonstrate that the system undergoes the layering transition connected with the condensation of the second layer on top of the dense floating solid. The density of the second layer is approximately the same as the density of the incommensurate monolayer. Thus, one can anticipate that the second layer should have a structure similar to the dense monolayer solid. Indeed, a direct inspection of the equilibrium configurations for the second layer confirms this assumption. An example of the bilayer configuration at $T^*=0.15$ is shown in Fig. 4, where the size of adsorbate atoms has been reduced for a better display. It should be noted

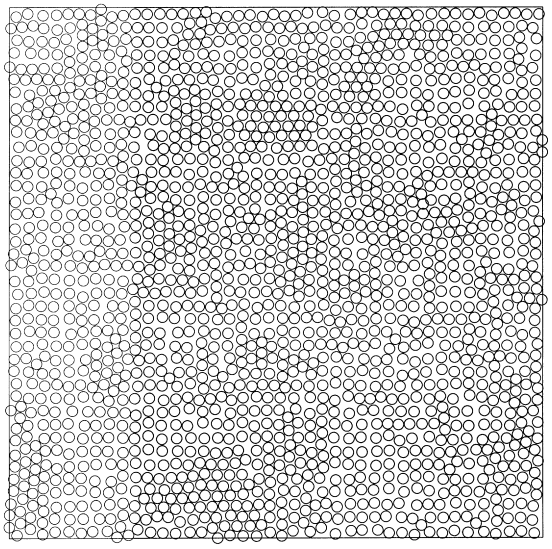

Fig. 3. Snap-shot configuration recorded at $T^*=0.3$ and $\mu^*=-7.5$. The system size is $40\times40\times10$ and contains 1845 particles.

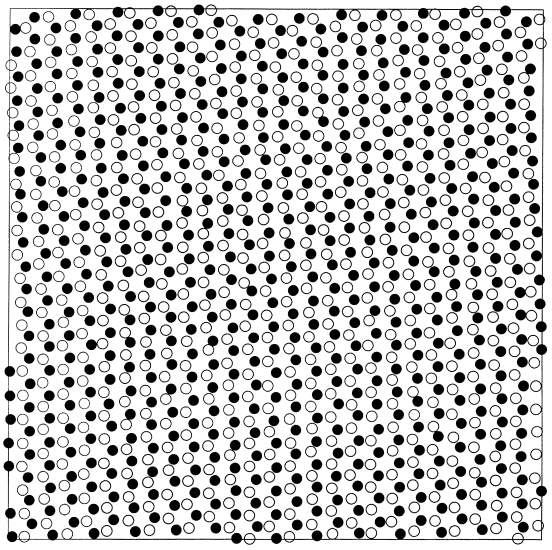

Fig. 4. Snap-shot configuration of bilayer film recorded at $T^*=0.15$ and $\mu^*=-6.40$. Open and filled circles represent particles adsorbed in the first and the second layers respectively.

that the presence of the second layer causes characteristic changes in the geometrical structure of the first layer. Fig. 5 shows the density profiles corresponding to the dense monolayer and the bilayer films at $T^*=0.15$ and at a chemical potential $\mu^*=$

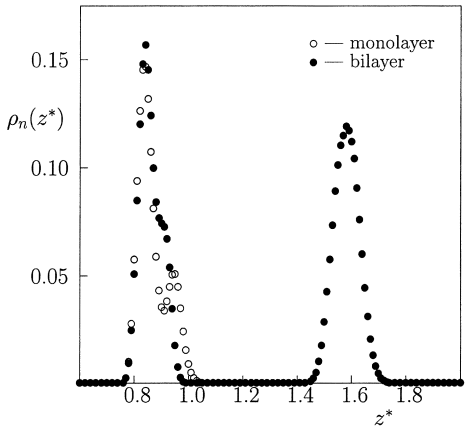

Fig. 5. Density profiles obtained for $T^*=0.15$ and $\mu^*=-7.2$ at both sides of the commensurate–incommensurate transition.

-7.2, i.e. just at the point of the layering transition. The second maximum in the density profile for the first layer, clearly seen for the monolayer film, is shifted towards shorter distance from the surface in the case of the bilayer film. From the analysis of Voronoi polygons, we have found that the monolayer is contracted due to the presence of the second layer. The average nearest neighbour distances in the dense monolayer and in the first layer of the bilayer film (at $T^*=0.15$) are equal to about 0.9 and 0.89 respectively. Also, the average misfit of the first layer changes from 16.37% in the monolayer film to about 17.38% in the bilayer film. The inspection of configurations generated during the simulation shows that the rotation of the adsorbed monolayer and bilayer with respect to the surface lattice changes slightly when the second layer is formed. The observed contraction of the nearest neighbour distance in the first layer due to the presence of the second layer (equal to about $0.01a$) is considerably greater than that deduced from theoretical calculations [51] for hexagonal films formed on a flat surface. Our finding can be readily explained by considering the changes in the density profiles shown in Fig. 5. In the monolayer film considerable numbers of particles assume positions with greater distances from the surface. In the case of the bilayer film, those particles are pushed towards the surface. Also, it should be noted that the integration of the density profiles allows us to estimate the densities in both layers. Such calculations have demonstrated that the first adsorbed layer density changes slightly when the second layer is formed on top of it. In the monolayer films we have estimated the upper limit of the incommensurate solid phase density as equal to about 1.44, whereas in the first layer of the bilayer film the upper limit of the first layer density is slightly higher and equal to 1.465.

Our central result is the phase diagram for the system considered here, which is presented in Fig. 6. Fig. 6a shows the phase diagram in the plane (ρ_n, T^*), and Fig. 6b in the plane (μ^*, T*). The data presented in Fig. 6a include the results of GCMC (filled circles) and CMC (stars and diamonds) simulations. In the case of CMC calcu-

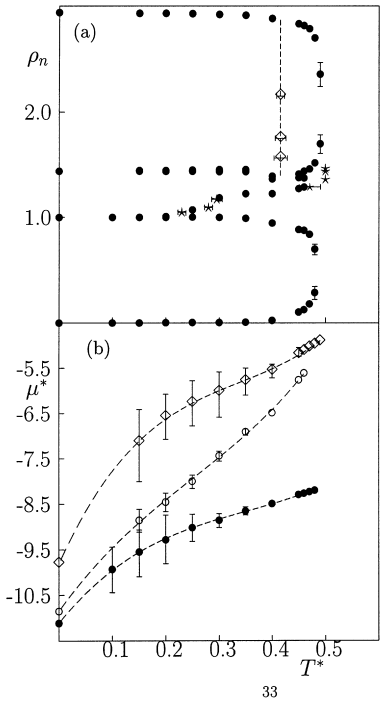

Fig. 6. Phase diagram for the system studied. (a) Phase diagram in the plane (T^*, ρ_n). Filled points are the results of GCMC calculations, and stars and diamonds correspond to the results for the first and the second layer, obtained from the CMC calculations. The triple line of the solid–fluid–gas coexistence in the second layer is shown as a broken vertical line. (b) The phase diagram in the (T^*, μ^*) plane obtained from the GCMC calculations (the gas – (1×1) transition points – ●; the (1×1) – floating solid transition points – ○; and the second layer condensation – ◇.

lations the locations of transition points have been estimated using the heat capacity changes with temperature (Fig. 7). The observed heat capacity peaks are rather small for monolayer films of density well below the density of an incommensurate solid phase, but become very sharp and high for denser films. The heat capacity maxima associated with the melting of the second layer have been found to become more pronounced and sharp as the film density increases. Nevertheless, the estimated melting temperature has been found to be constant and equal to about 0.415. Another interesting result is the constancy of the melting temperature for the first layer, when the total film density is close to, or higher than, the upper limit of the incommensurate phase density. Under such conditions, the monolayer melts at $T^* \approx 0.5$, as is demonstrated by the results of heat capacity calculations given in Fig. 7.

We have not been able to perform reliable calculations for the commensurate–incommensurate transition as well as for the condensation of the second layer at very low temperatures, below $T^* = 0.15$. Also, we have not attempted any direct ground-state calculations for the dense incommensurate monolayer and the bilayer structures.

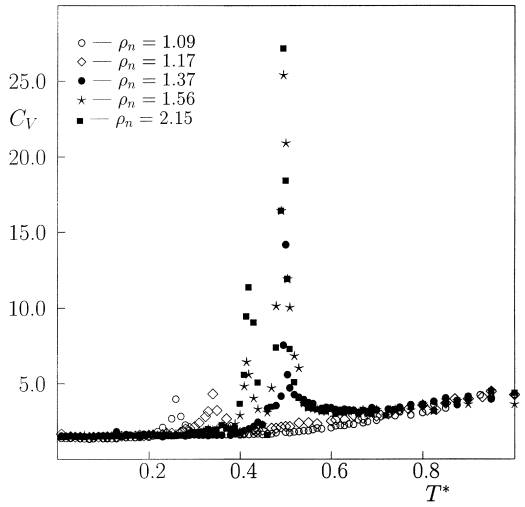

Fig. 7. The heat capacity curves for systems of different density obtained from the canonical ensemble Monte Carlo simulation ($M = 20$).

Therefore, the extrapolation of the results to $T^* = 0$, shown in Fig. 6b, is quite uncertain. It should be noted that the detailed ground state analysis of such a system is very difficult. A simple 2D model is inadequate and cannot lead to a reasonable estimation of the stable configurations for all phases. Only in the case of the dilute 2D gas and the registered (1×1) phases is it easy to calculate the energy and the grand canonical potential at zero temperature. Large out-of-plane effects present in the incommensurate phase make the estimation of the ground-state properties a nontrivial problem. Also, the application of the Novaco–McTague theory [42,43], in order to estimate the rotation of the adsorbed monolayer with respect to the surface lattice, is not easy owing to large out-of-plane effects. In the case of a bilayer the problem becomes still more complex.

The transition between the dilute 2D gas and the registered (1×1) phase occurs at $T^* = 0$ at a chemical potential $\mu^* \approx -11.2151$. This results simply from the known energies (per unit area) of both phases, equal to 0.0 and -11.2151 respectively.

We have attempted to estimate the location of the commensurate–floating solid incommensurate transition at zero temperature using the results of the Monte Carlo simulation in the canonical ensemble. To do so, the low temperature MC calculations for systems of different densities ranging from $\rho_n = 1.0$ to 1.5625 have been performed. The upper limit of the system density used is already well above the monolayer capacity, estimated from the GCMC calculations as equal to about 1.44. The canonical ensemble simulation has confirmed the above result very nicely. Fig. 8 shows the changes in the first and the second layer densities ($\rho_n(i)$, $i = 1, 2$) versus temperature for a series of systems with different total density (shown in the figure). It is evident that in the case of total density equal to 1.5625, the first layer has a density of about 1.44, and the excess of adsorbed particles is located in the second layer. For the densities below ρ_n^m, the system exhibits the coexistence of the commensurate and incommensurate phases. The data presented in Fig. 8 also illustrate changes in the mechanism of melting in the first layer. When the film density is considerably lower than

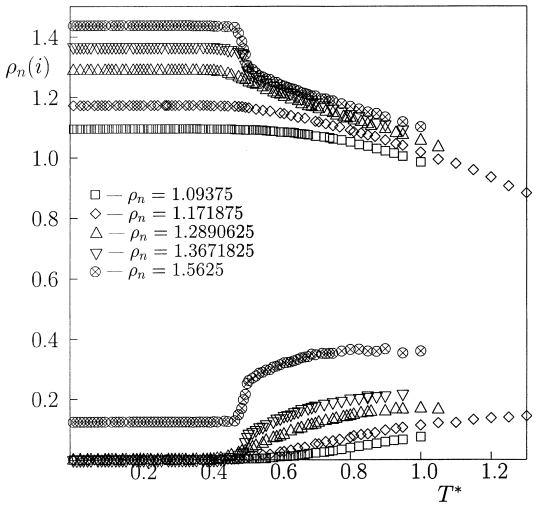

Fig. 8. Temperature changes in the densities of the first and the second layers in systems of different density (shown in the figure).

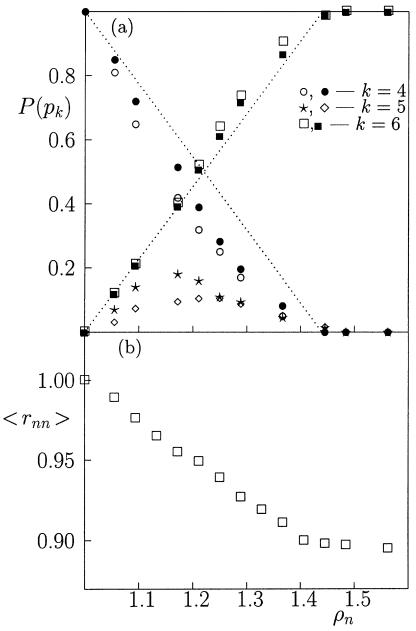

Fig. 9. Density changes of the contributions of different Voronoi polygons (a) and the average nearest neighbour distance (b) at $T^*=0$, obtained by extrapolation of simulations carried out at low temperatures. The results in (a) have been obtained for systems of size $M=20$ (○, ★, □) and $M=40$ (●, ◇, ■). Dotted lines correspond to the predicted contributions of the registered and incommensurate phases in the macroscopic system and are calculated from Eq. (6). The results shown in (b) correspond to the system with $M=40$.

the monolayer capacity, melting does not cause any change in the first layer density. On the other hand, melting of denser films is accompanied by a sudden transfer of a certain number of adsorbed particles from the first to the second layer.

Concluding, we would like to comment some more on the behaviour of monolayer films at intermediate densities. Fig. 9 presents the changes in the contributions of different Voronoi polygons and the average nearest neighbour distance in the first adsorbed layer versus total film density. The results presented above have been obtained from the canonical ensemble MC simulations performed at very low temperatures between 0.01 and 0.1. Under such conditions the film structure was very stable. In particular, the distributions of the Voronoi polygons have not shown any systematic changes (for a given film density), so that the results presented in Fig. 8 correspond to averages taken over the above-mentioned temperature range. Our results are consistent with the two-phase coexistence picture, assuming that the system consists of regions formed by the registered phase, of number density equal to 1.0, and regions of the FIC phase of density equal to 1.44. The fraction of the surface corresponding to the registered (1×1) phase and the fraction corresponding to the hexagonal close packed phase can be roughly estimated as being equal to the contributions of the Voronoi tetragons and hexagons respectively. The data obtained for two different system sizes show that the contribution of pentagons becomes lower when the system size increases. This can be attributed to the fact that in a larger system the interfacial region becomes increasingly less important, with respect to the contributions of both coexisting phases. In the truly macroscopic system one can expect that the interfacial region should give a negligible contribution. Thus, assuming that the fraction of the system space occupied by the registered (1×1) phase is equal to x_r, the fraction of the system space occupied by the incommensurate solid should be equal to $(1-x_r)$. One can estimate x_r from the simple linear equation

$$\rho_n^1 = 1.0x_r + (1-x_r)1.44 \qquad (6)$$

The contributions of both coexisting phases, predicted from Eq. (6) are also been shown in Fig. 9 (dashed lines). In the macroscopic system the contribution of the Voronoi tetragons can be used as a direct measure of x_r. The results presented in Fig. 9 are quite consistent with the above prediction.

The two-phase coexistence in monolayer films can be very nicely confirmed by studying the behaviour of the block density distribution functions. Fig. 10 presents the results obtained for the system with total density $\rho_n \approx 1.11$ at two different temperatures $T^* = 0.20$ and $T^* = 0.5$. Despite a large statistical effort to sample the density probability distribution (4×10^{10} Monte Carlo moves), the results for $T^* = 0.2$ are still rather poor. In particular, on the side of high density phase there is much spurious structure present. Nevertheless, it is clear that the system is in the region of two-phase coexistence at $T^* = 0.2$ and in the one-phase region at $T^* = 0.5$. Unfortunately, the limited quality of the results at low temperatures excludes any possibility of reliable moment analysis [60].

Finally, we would like to call the reader's attention to some interesting property of the system studied here. Namely, at very low temperatures, well below the monolayer melting point, the potential energy per particle is nearly the same in both solid phases (see Fig. 11a). Of course, the contributions resulting from the admolecule–admolecule and the admolecule–substrate interactions change with the density, due to changes in the fraction of the surface covered by both solid phases. In Fig. 11b we show the gas–substrate contributions to the total energy and find that at low temperatures $\langle e_{gs} \rangle$ changes linearly with the film density. This is demonstrated in the inset in Fig. 11b, where we have plotted the gas–solid energy versus film density at $T^* = 0.0$, obtained by extrapolation of data for finite temperatures. From the results shown in Fig. 11 it follows that at sufficiently low temperature, when the entropic effects are very small, the free energy barrier that must be overcome for the system to change its state is also very low. The above results are consistent with the considered earlier changes in the contributions of both solid phases with density.

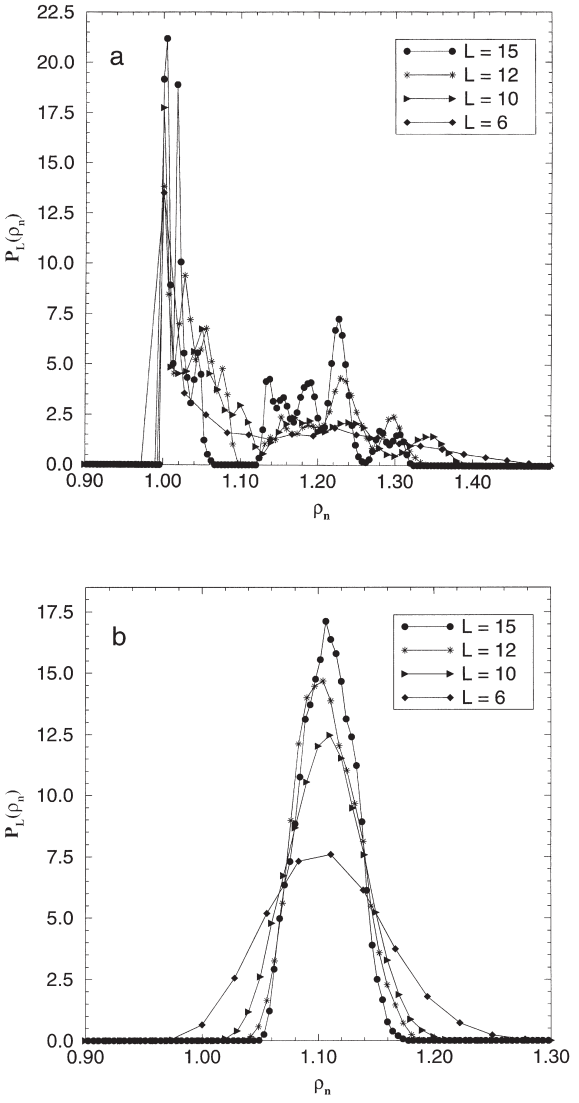

Fig. 10. The block density distribution functions obtained for a system with $M = 60$ at $T^* = 0.2$ (a) and $T^* = 0.5$ (b). The block sizes L are shown in the figure.

5. Summary and final remarks

We have performed an extensive Monte Carlo study of phase transitions in model monolayer and bilayer films formed on the (100) plane of an fcc crystal. In the system considered in this work the monolayer film exhibits three different phases at low temperatures, depending on the density of the adsorbed layer. At the low density limit we have

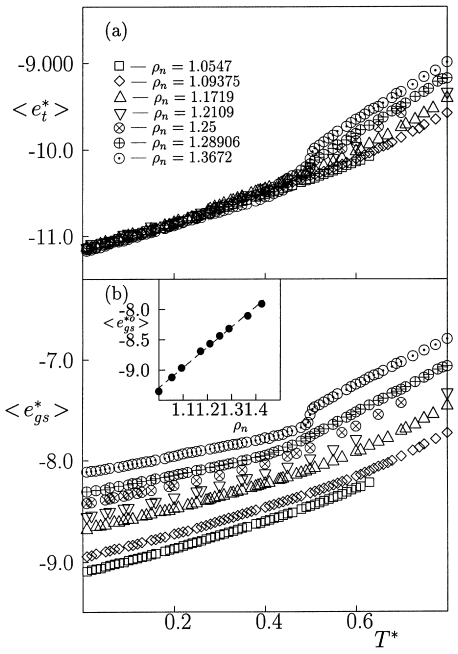

Fig. 11. Changes of the total average energy per particle (a) and of the average adsorbate–substrate energy per particle (b) versus temperature for systems of different densities. The inset shows the gas–solid energy versus film density, extrapolated to $T^* = 0.0$.

the 2D gas phase. As the density increases, the registered (1×1) phase of the density $\rho_n = 1.0$ is formed. Further increase in the film density leads to the formation of the incommensurate solid phase. The melting of the monolayer solid phase has been found to depend strongly on the film density. In the submonolayer regime, the solid–fluid transition is associated with a sudden disordering of the film and this process is not accompanied by desorption or promotion of the second layer. On the other hand, the melting of the dense incommensurate monolayer leads to a decrease of the first layer density, due to the promotion of the second layer. The melting temperature of submonolayer films increases with the density until the monolayer reaches its capacity. The melting of the first adsorbed layer in films with a partially filled second layer occurs at an approximately constant temperature of $T^* \approx 0.5$. Our results are consistent with experimentally observed changes in the melting mechanism in the nitrogen films on graphite (for a review, see Ref. [63]), as well as with the results of computer simulations for methane films on graphite [64] and argon films on MgO [65].

In the temperature range considered in this paper the formation of the second layer has been found to occur only after the completion of the first layer. At low temperatures, the second layer assumes the same structure as the high density monolayer solid phase. The melting transition in the second layer occurs at the constant (density independent) temperature of about $T^* = 0.42$. Taking into account that the triple point of the 2D Lennard–Jones fluid occurs at $T^* \approx 0.4$ [66], we conclude that the second layer melting is only slightly perturbed by the nonuniformity of the potential field exerted by the solid substrate and the first adsorbed layer.

An interesting and still open question is the nature of the adsorbate lattice distortion leading to the rotation of the incommensurate monolayer with respect to the substrate lattice. In general, such effects may be due to temperature fluctuations, local elastic relaxations, the presence of defects and vacancies, and finite size effects, as well as possibly resulting from the shape of the simulation cell. It is possible that there exist several intermediate (high-order commensurate) phases between the low density registered phase and the high density incommensurate solid phase.

Acknowledgements

This work has been partially supported by the Volkswagen Foundation (grant No. 1/71809). A grant for computer time from the ICM (Warsaw University, Poland) is also gratefully acknowledged.

References

[1] J.G. Dash, Films on Solid Surfaces, Academic Press, New York, 1975.
[2] A. Thomy, X. Duval, J. Regnier, Surf. Sci. Rep. 1 (1981) 1.
[3] M. Schick, Prog. Surf. Sci. 11 (1981) 254.
[4] A. Patrykiejew, S. Sokołowski, Adv. Colloid Interface Sci. 30 (1989) 203.
[5] H.-J. Freund, Ber. Bunsenges. Phys. Chem. 99 (1995) 1261.

[6] K. Binder, in: C. Domb, J.L. Lebowitz (Eds.), Phase Transitions and Critical Phenomena 8 , Academic Press, London, 1983, p. 1.
[7] C. Uebing, Surf. Sci. 272 (1992) 247.
[8] N.C. Bartelt, L.D. Roelofs, T.L. Einstein, Surf. Sci. 221 (1989) L750.
[9] A.N. Berker, S. Ostlund, F.A. Putnam, Phys. Rev. B 17 (1978) 3650.
[10] A. Patrykiejew, in: A. Dąbrowski, V.A. Tertykh (Eds.), Adsorption on New and Modified Inorganic Sorbents, Elsevier, Amsterdam, 1996.
[11] B.N.J. Persson, Surf. Sci. 258 (1991) 451.
[12] J.W. Cahn, J. Chem. Phys. 66 (1977) 3667.
[13] R. Evans, in: D. Henderson (Ed.), Fundamentals of Inhomogeneous Fluids, Marcel Dekker, New York, 1992.
[14] S.D. Prasad, S. Toxvaerd, J. Chem. Phys. 74 (1981) 6431.
[15] D. Henderson, in: D. Henderson (Ed.), Fundamentals of Inhomogeneous Fluids, Marcel Dekker, New York, 1992.
[16] D. Henderson, F.F. Abraham, J.A. Barker, Mol. Phys. 42 (1981) 767.
[17] T. Meichel, J. Suzanne, C. Girard, C. Girardet, Phys. Rev. B 38 (1988) 3781.
[18] O.E. Vilches, Annu. Rev. Phys. Chem. 31 (1980) 463.
[19] J. Cui, S.C. Fain Jr., H. Freimuth, H. Wiechert, H.P. Schildberg, H.J. Lauter, Phys. Rev. Lett. 60 (1988) 1848.
[20] J. Villain, in: T. Riste (Ed.), Ordering in Strongly Fluctuating Condensed Matter Systems, Plenum Press, New York, 1980.
[21] M.H.W. Chan, in: H. Taub, G. Torzo, H.J. Lauter, S.C. Fain Jr., (Eds.), Phase Transitions in Surface Films 2, Plenum Press, New York, 1991, p. 1.
[22] K. Kern, C. Comsa, in: H. Taub, G. Torzo, H.J. Lauter, S.C. Fain Jr., (Eds.), Phase Transitions in Surface Films 2, Plenum Press, New York, 1991, p. 41.
[23] F.F. Abraham, W.E. Rudge, D.J. Auerbach, S.W. Koch, Phys. Rev. Lett. 52 (1984) 445.
[24] M. Grunze, P.H. Kleban, W.N. Unertl, F.S. Rys, Phys. Rev. Lett. 51 (1983) 582.
[25] E.D. Specht, M. Sutton, R.I. Birgeneau, D.E. Moncton, P.M. Horn, Phys. Rev. B 30 (1984) 1589.
[26] J. Villain, Surf. Sci. 97 (1980) 219.
[27] F.D.M. Haldene, J. Villain, J. Phys. (Paris) 42 (1981) 1673.
[28] M. den Nijs, C. Domb, J.L. Lebowitz (Eds.), Phase Transitions and Critical Phenomena 12, Academic Press, London, 1991, p. 219.
[29] L.W. Bruch, Surf. Sci. 250 (1991) 267.
[30] M.B. Gordon, Phys. Rev. B 35 (1987) 2052.
[31] P.W. Stephens, P.A. Heiney, R.J. Birgeneau, P.M. Horn, Phys. Rev. Lett. 43 (1979) 47.
[32] P.W. Stephens, P.A. Heiney, R.J. Birgeneau, P.M. Horn, D.E. Moncton, C.S. Brown, Phys. Rev. B 29 (1984) 3512.
[33] F.C. Motteler, J.G. Dash, Phys. Rev. B 31 (1985) 346.
[34] A. Marx, Phys. Rep. 125 (1985) 1.
[35] E.D. Specht, A. Mak, C. Petters, M. Sutton, R.J. Birgeneau, K.L. D'Amico, D.E. Moncton, S.E. Nagler, P.M. Horn, Z. Phys. B 69 (1987) 347.
[36] S.C. Fain, M.D. Chinn, R.D. Diehl, Phys. Rev. B 21 (1980) 4170.
[37] K. Kern, R. David, P. Zeppenfeld, R. Palmer, G. Comsa, Solid State Commun. 62 (1987) 391.
[38] L.W. Bruch, J.A. Venables, Surf. Sci. 148 (1984) 167.
[39] C. de Beauvais, D. Rouxel, B. Mutaftschiev, B. Bigeard, Surf. Sci. 272 (1992) 73.
[40] B.M. Ocko, O.M. Magnussen, J.X. Wang, Th. Wandlowski, Phys. Rev. B 53 (1996) R7654.
[41] D.R. Nelson, B.I. Halperin, Phys. Rev. B 19 (1979) 2457.
[42] A.D. Novaco, J.P. McTague, Phys. Rev. Lett. 38 (1977) 1286.
[43] J.P. McTague, A.D. Novaco, Phys. Rev. B 19 (1979) 5299.
[44] C.G. Shaw, S.C. Fain Jr., M.D. Chinn, Phys. Rev. Lett. 41 (1978) 955.
[45] C. Calisti, J. Suzanne, Surf. Sci. 105 (1981) L255.
[46] A. Patrykiejew, S. Sokołowski, T. Zientarski, Langmuir 13 (1997) 1036.
[47] B.I. Halperin, D.R. Nelson, Phys. Rev. Lett. 41 (1978) 121.
[48] K.J. Strandburg, Rev. Mod. Phys. 60 (1988) 161.
[49] A. Patrykiejew, S. Sokołowski, T. Zientarski, K. Binder, J. Chem. Phys. 102 (1995) 8221.
[50] L.W. Bruch, M.S. Wei, Surf. Sci. 100 (1980) 481.
[51] M.S. Wei, L.W. Bruch, J. Chem. Phys. 75 (1981) 4130.
[52] W.A. Steele, Surf. Sci. 36 (1973) 317.
[53] H.-Y. Kim, W.A. Steele, Phys. Rev. B 45 (1992) 6226.
[54] D.J. Adams, Mol. Phys. 28 (1974) 1241.
[55] D.J. Adams, Mol. Phys. 29 (1975) 307.
[56] J. Yao, R.A. Greenkorn, K.C. Chao, Mol. Phys. 46 (1982) 587.
[57] M. Tanemura, T. Ogawa, N. Ogita, J. Comput. Phys. 51 (1983) 191.
[58] K. Binder, Z. Phys. B 43 (1981) 119.
[59] M. Rovere, D.W. Heermann, K. Binder, Europhys. Lett. 6 (1988) 585.
[60] M. Rovere, D.W. Heermann, K. Binder, J. Phys.: Condens. Matter 2 (1990) 7009.
[61] L.P. Kadanoff, in: C. Domb, M.S. Green (Eds.), Phase Transitions and Critical Phenomena, vol. 5a, Academic Press, London, p. 1.
[62] E. Vives, P.A. Lindgård, Phys. Rev. B 47 (1993) 7431.
[63] D. Marx, H. Wiechert, Adv. Chem. Phys. 95 (1996) 213.
[64] J.M. Phillips, C.D. Hruska, Phys. Rev. B 39 (1989) 5425.
[65] A. Alavi, I.R. McDonald, Mol. Phys. 69 (1990) 703.
[66] J.M. Phillips, L.W. Bruch, R.D. Murphy, J. Chem. Phys. 75 (1981) 5097.